recycling

MDPI

Article

Recycled Glass and Plastic Waste in Sustainable Geopolymer Systems for Affordable Housing Solutions

Zhao Qing Tang [1], Yat Choy Wong [2,*], Yali Li [1] and Eryadi Kordi Masli [3]

[1] Centre for Smart Infrastructure and Digital Construction, School of Engineering, Swinburne University of Technology, Hawthorn, VIC 3122, Australia; ztang@swin.edu.au (Z.Q.T.); yalili@swin.edu.au (Y.L.)
[2] Department of Mechanical and Product Design Engineering, School of Engineering, Hawthorn, VIC 3122, Australia
[3] Department of Business, Technology and Entrepreneurship, School of Business, Law and Entrepreneurship, Hawthorn, VIC 3122, Australia; emasli@swin.edu.au
* Correspondence: ywong@swin.edu.au

Abstract

The increasing demand for sustainable construction materials has driven research into low-carbon geopolymers that mitigate both cement-related emissions and plastic and glass waste accumulation. This study explores the development of geopolymer concrete incorporating fly ash (FA), slag (S), and FA + S blends, with 10% recycled crushed glass (RCG) and recycled plastic waste (RPW) as partial coarse aggregate replacements. Compressive strength testing revealed that FA + S-based geopolymers (25FA + S) with 100% ordinary Portland cement (OPC) replacement achieved a 7-day strength of 24.6 MPa, representing a 98% improvement over control specimens. Slag-based geopolymers demonstrated water absorption properties comparable to OPC, indicating enhanced durability. Microstructural analyses using SEM, XRD, and EDS confirmed the formation of a dense aluminosilicate matrix, with slag promoting FA reactivity and reinforcing interfacial transition zone (ITZ). These effects contributed to superior mechanical performance and water resistance. Despite minor shrinkage-induced cracking, full OPC replacement with S or FA + S geopolymers outperformed control specimens, consistently exceeding the target strength of 15 MPa required for low-impact, single-story housing applications within seven days. These findings underscore the potential of geopolymer systems for rapid and sustainable construction, offering an effective solution for reducing carbon footprints and repurposing industrial waste.

Keywords: recycled plastic; recycled crushed glass; green concrete; geopolymer; microstructure; interfacial transition zone

Academic Editor: Francesco Paolo La Mantia

Received: 6 June 2025
Revised: 18 July 2025
Accepted: 25 July 2025
Published: 27 July 2025

Citation: Tang, Z.Q.; Wong, Y.C.; Li, Y.; Masli, E.K. Recycled Glass and Plastic Waste in Sustainable Geopolymer Systems for Affordable Housing Solutions. *Recycling* **2025**, *10*, 147. https://doi.org/10.3390/recycling10040147

1. Introduction

In recent years, house demanding has been rising rapidly, a trend that is particularly problematic in developing countries experiencing significant population growth [1–3]. In nations such as Indonesia, Nigeria, and Bangladesh, where a large portion of the population lives on low incomes and population growth is high, the challenge of accessing affordable housing is becoming more acute, and low-cost housing policies have been pursued [4–8]. Beyond external factors that are difficult to control, such as global economic trends and market fluctuations, one of the primary drivers of high housing costs is the price of building materials accounting for up to 80% of the total cost of a basic residential unit [9]. Therefore, using alternative raw materials—particularly waste-derived resources requiring minimal

processing—offers an economically and environmentally sustainable solution for residents, governments, and the construction industry.

The construction industry significantly contributes to greenhouse gas emissions and global warming, with Portland cement production alone accounting for 5–7% of global anthropogenic CO_2 emissions [10]. These emissions are expected to rise with future infrastructural growth driven by population increases. Geopolymer cement, a greener alternative, is produced by reacting an aluminosilicate source (e.g., fly ash, metakaolin) with a concentrated alkali hydroxide or silicate solution [11]. Unlike ordinary Portland cement (OPC), geopolymer materials require about 50% less energy for production and can reduce the carbon footprint by up to 80% in favorable conditions [12]. This is largely because its ingredients can be sourced from industrial waste by-products such as fly ash or slag [13]. In addition to its environmental benefits, geopolymer cement has also been shown to be cost-effective compared to OPC in some cases, particularly when industrial by-products are used as primary precursors. For instance, Akhtar et al. (2022) performed a cost comparison between geopolymer concrete and conventional concrete and found that geopolymer concrete had lower production cost ($\$73.70/m^3$ vs. $\$81.65/m^3$ for conventional concrete mix following Bureau of Indian Standard) despite requiring specialized activators, due to the elimination of cement and efficient use of industrial by-products [14]. Similarly, Rintala et al. (2021) reported that waste-based blended geopolymeric materials significantly reduced costs when considering carbon taxes, transport reductions, and long-term lifecycle benefits [15]. These findings reinforce the premise that geopolymer technology, especially when integrated with municipal and industrial waste streams, presents a compelling case for both environmental sustainability and financial viability in construction applications. Thus, adopting a waste reuse approach in geopolymer binder systems aligns more effectively with the goals of (i) promoting green and sustainable practices, (ii) providing cost-effective construction alternatives that address both carbon taxes and sustainability concerns, and (iii) facilitating more affordable housing solutions.

The potential for glass waste reuse in construction materials has received increasing attention. Researchers have explored using glass waste as a supplementary cementitious material (SCM) and as a partial replacement for cement due to its pozzolanic properties [16]. In geopolymer systems, waste glass serves as a substitute for other aluminosilicate powders, such as metakaolin, owing to its high concentration of amorphous silica, which can also be utilized to produce alkaline activators [17,18]. However, the incorporation of glass in cementitious systems requires careful consideration of expansion and cracking issues caused by alkali-silica reaction (ASR). To mitigate these risks, glass typically needs to be used in small percentages to avoid detrimental impacts on the concrete matrix. Additionally, optimizing the performance of glass waste as a raw precursor in cementitious systems often involves expensive and intricate treatment processes, such as high-temperature calcination, which demand significant energy and can be less favorable from economic and sustainability perspectives [19,20]. Using glass waste as crushed aggregate to replace coarse natural aggregates aligns more closely with the scope of this study, offering a more practical and less energy- and cost-intensive approach compared to the production of finely ground glass powder. Although coarse glass aggregates present a higher risk of ASR compared to fine aggregates [16], the incorporation of supplementary cementitious materials such as slag or fly ash (FA), or the adoption of alkali-activated/geopolymer binder systems, has been shown to more effectively suppress ASR-related durability issues than conventional OPC-based systems [21,22]. Therefore, the use of glass waste as coarse aggregate, when combined with geopolymer binders, represents a more viable, durable, and sustainable solution for glass waste valorization in the construction industry.

Plastic waste is a growing global issue. Using Indonesia as an example, it contributes 4% of global plastic waste as of 2020, projected to reach 15% by 2025 [23]. Poor waste management exacerbates the problem—on Java Island, only 11.83% of urban plastic waste is recycled, while 88.17% ends up in landfills or the environment [24]. This leads to severe environmental, economic, and health consequences, including threats to biodiversity, increased landfill costs, and microplastic contamination in the food chain [25,26]. However, plastic waste presents an untapped economic opportunity. Recent research explores its potential use in construction materials, particularly in Portland cementitious systems, offering a promising approach to repurposing waste into valuable resources [27,28]. Concrete incorporating plastic waste often results in low performance [29,30]. For example, according to Luis et al., incorporating 7.5% plastic aggregates can reduce the compressive strength of concrete by approximately 40–50% in the worst-case scenario [30]. Conversely, the use of glass aggregates typically enhances concrete performance but is limited due to potential alkali-silica reaction (ASR) risks when used in large quantities. Thus, combining plastic and glass aggregates may offer a balanced approach, leveraging complementary advantages while minimizing individual drawbacks. Earlier work [30,31], demonstrated that the mechanical properties of concrete incorporating plastic and glass waste as partial aggregate replacements were comparable to those of standard concrete [31,32]. This approach shows significant potential for advancing sustainable recycling of plastic and glass waste in concrete production. However, since ordinary Portland cement (OPC) was the primary binder in that study, its environmental impact remains a concern, given that OPC is one of the largest contributors to greenhouse gas emissions in conventional concrete production. Consequently, the sustainability benefits of that approach were limited by the carbon footprint of the binder. In fact, despite the advantages of utilizing plastic and glass waste and the well-established benefits of geopolymer systems, research integrating multiple waste-derived aggregates into a single geopolymer matrix remains limited, restricting the full realization of sustainability potential in construction materials.

In the present study, we aim to address this limitation by investigating the feasibility of using a combination of non-biodegradable crushed glass and plastic aggregates in a geopolymer concrete system, wherein OPC is entirely replaced with industrial by-products such as slag and fly ash. Crushed glass aggregates in geopolymer matrices can chemically react with alkaline activators (e.g., NaOH or Na_2SiO_3), initiating pozzolanic reactions that form additional C–A–S–H (calcium aluminosilicate hydrate—a binding gel similar to C–S–H but with partial substitution of Si by Al, commonly found in high-calcium geopolymer systems) or N–A–S–H gels (sodium aluminosilicate hydrate, the primary geopolymer gel) at the interface—an effect less pronounced in OPC systems. While plastic aggregates are generally inert and bond poorly with OPC, the highly alkaline environment of geopolymer binders can induce mild surface etching or micro-mechanical anchoring on treated plastic surfaces, slightly improving adhesion. This substitution aims to enhance sustainability and utilize cost-effective waste materials, aligning with the low-cost housing goals in developing countries, without very much compromising on the necessary durability and strength. While previous studies have explored geopolymer systems with industrial by-products, limited research has focused on the synergistic effects of mixed plastic and glass aggregates within these matrices. This study fills this gap by investigating how their inclusion influences geopolymerization kinetics and phase composition. A key aspect is understanding the interaction mechanisms, microstructural transformations, and phase evolution within the modified binder system. Additionally, it is crucial to assess the performance of the newly developed binder formulation, particularly its ITZ behavior, microstructural integrity, and durability. To achieve this, SEM-EDS and XRD analyses were conducted to characterize the morphological and compositional changes, as well

as ITZ characteristics between the binder and aggregates. Furthermore, compressive strength and water absorption tests were performed to evaluate mechanical integrity and transport properties.

With compressive strength requirements for single-story housing typically ranging from 10 to 15 MPa [9], this research aims to develop a geopolymer concrete that meets these structural benchmarks while also mitigating reliance on natural sand. This is particularly beneficial for countries experiencing severe sand shortages due to rapid infrastructure expansion and resource depletion, as seen in Singapore and India [33]. By valorizing plastic and glass waste into high-performance construction materials, this study contributes to advancing circular economy principles, reducing environmental burden, and promoting cost-effective, sustainable alternatives to traditional concrete.

2. Materials and Method

2.1. Materials

In this study, plastic waste was collected from household sources in Melbourne, Australia. The recycled plastic waste (RPW) was shredded and prepared for use in concrete mixtures. Recycled waste glass was obtained from a local recycling company in Victoria, primarily consisting of glass from bottles and jars collected through domestic kerbside recycling. Gravel and river sand were used as coarse and fine aggregates, respectively. The recycled crushed glass (RCG) was processed to produce aggregates with an average diameter of 5.5 mm to match that of the river sand aggregates. The particle size graduation was verified by sieve analysis to ensure consistency with the control specimens, thereby minimizing any grading-induced variability. Ordinary Portland Cement (OPC), ground granulated blast furnace slag (S), and low-calcium Class F fly ash (FA) were sourced locally from commercial suppliers. The chemical compositions of crushed glass and cement powder (Tables 1 and 2), as well as slag and fly ash (Tables 3 and 4), were determined using X-ray fluorescence (XRF) analysis. Alkali activation was achieved using sodium silicate solution (Grade D, PQ Australia) with a SiO_2:Na_2O molar ratio of 2.0, along with 8 M sodium hydroxide (NaOH) solution, prepared by dissolving NaOH beads (98%, Sigma-Aldrich) in deionized water.

Table 1. Bulk oxide components (wt.%) of RCG.

Compound	Al_2O_3	SiO_2	CaO	Fe_2O_3	K_2O	SO_3	Na_2O	MgO	LOI
%	1.38	72.6	11.7	0.5	0.4	0.1	13.1	0.6	0.22

LOI: loss on ignition at 1000 °C.

Table 2. Bulk oxide components (wt.%) of OPC.

Compound	Al_2O_3	SiO_2	CaO	Fe_2O_3	K_2O	SO_3	Na_2O	MgO	L.O.I.
%	4.5	20.3	62.9	4.6	0.3	2.6	0.3	1.2	3.3

LOI: loss on ignition at 1000 °C.

Table 3. Bulk oxide components (wt.%) of Slag.

Compound	Al_2O_3	SiO_2	CaO	Fe_2O_3	K_2O	TiO_2	Na_2O	MgO	L.O.I.
%	12.4	32.6	45.06	0.25	0.28	0.57	0.25	5.4	3.19

LOI: loss on ignition at 1000 °C.

Table 4. Bulk oxide components (wt.%) of Fly ash.

Compound	Al_2O_3	SiO_2	CaO	Fe_2O_3	K_2O	TiO_2	Na_2O	MgO	L.O.I.
%	18.6	70.7	1.95	2.82	1.50	0.75	0.48	0.43	2.77

LOI: loss on ignition at 1000 °C.

2.2. Sample Preparation

The coarse gravel aggregate, river sand, RPW, and RCG were oven-dried at 105 °C for 24 h before use. The coarse aggregates used in this study had a particle size range of 5–19 mm, while RPW and RCG had an average particle size of approximately 5.5 mm. River sand was used as the fine aggregate component in the concrete mixtures. It should be noted that the particle size distribution (PSD) of the replacement materials differed slightly from that of the natural aggregates: the RPW and RCG particles were coarser than river sand but finer than the original coarse aggregates. Despite this variation, the total aggregate volume and the binder-to-aggregate ratio were kept constant across all mixtures to ensure mix consistency and preserve the overall packing density. This approach allowed for a reliable comparison of material performance, with minimal influence from gradation-related variability. A mixed Na_2SiO_3 and NaOH solutions were used as a liquid alkaline activator for the activation of FA, S, and a binary precursor (FA + S) with a fixed FA:S ratio of 50:50. A fixed Na_2SiO_3:NaOH ratio of 70:30, and an activator/precursor ratio of 0.4, were adopted in this project. The molarity of the NaOH solution was kept constant at 8 mol in this project. Different proportions of coarse aggregate, river sand, RPW, RCG, along with geopolymers or cement and a desirable amount of superplasticizer, were mixed and housed into a standard-sized mould (100 mm in diameter and 200 mm in height) to prepare samples for the unconfined compressive strength (UCS) measurements. The samples were demoulded after 24 h and further cured in a humidity chamber at room temperature for the testing age of 7 and 28 days. Ambient curing was intentionally selected to minimize energy consumption and align with the study's focus on developing practical and low-cost construction method, particularly in resource-constrained settings. The control mix design adopted a fixed binder-to-aggregate ratio of 25% across all mixtures. In the control specimen, 10% of the coarse aggregate volume in the M40 grade concrete mix [32] was replaced with RPW and RCG at a fixed RPW:RCG ratio of 50:50, where such design mix was chosen based on our earlier in-house trials and publications [32,34]. To explore more sustainable alternatives, the fixed 25% binder portion in each mix was composed of either 100% OPC (in the control) or a combination of OPC and alkali-activated precursors—fly ash (FA), slag (S), or a binary blend of FA and S (FA + S). Specifically, 10%, 15%, and 25% of the total concrete mix (i.e., 40%, 60%, and 100% of the binder fraction, respectively) were replaced with these precursors, representing increasing levels of OPC substitution. The binder-to-aggregate ratio remained constant at 25% across all mixtures. Aggregates and the cement precursor were first mixed in their dry form for 2–3 min until an even distribution and consistent coloration were achieved. Sodium hydroxide (NaOH) solution was then added, followed by sodium silicate (Na_2SiO_3) solution, maintaining a fixed Na_2SiO_3:NaOH ratio of 70:30 and an activator liquid/precursor ratio of 0.4. These ratios were selected based on their ability to achieve high strength in waste-reused geopolymer blends, as reported by Arul et al. [34]. After mixing for an additional 2 min, superplasticizer was added to enhance the workability of the concrete mixtures. After mixing, the concrete was cast into cylindrical molds with dimensions of 100 mm in diameter and 200 mm in height. The freshly cast specimens were left in the molds and placed in a humidity chamber (relative humidity > 95%) for 24 h before demolding to prevent moisture lost. Following demolding, the samples were further cured in a humidity chamber at room temperature for 7 and

28 days. Different concrete mixtures were produced according to the mix designs outlined in Table 5. Concrete cube specimens measuring 50 mm were prepared for water absorption testing.

Table 5. Mix design of concrete.

Mixes	ID	Total Binder Content
OPC only (control)	C	100% OPC
FA-geopolymer mix	10FA	40%FA + 60%OPC
	15FA	60%FA + 40%OPC
	25FA	100%FA
S-geopolymer mix	10S	40%S + 60%OPC
	15S	60%S + 40%OPC
	25S	100%S
(FA + S)-geopolymer mix	10FA + S	40%(FA + S) + 60%OPC
	15FA + S	60%(FA + S) + 40%OPC
	25FA + S	100%(FA + S)

Note: Aggregates in the mix design consisted of coarse aggregate + river sand + RPW+ RCG; water to solid ratio (w/s) was 0.4.

2.3. Performance Evaluation and Characterisation

UCS tests were performed following ASTM C39 using a 2000 kN Tecnotest compression testing machine, applying an axial strain rate of 0.5% per minute. Two replicates for 7-day curing samples and three replicates for 28-day curing ones were tested for each mix design, and the average value was reported.

Water absorption through capillary action was assessed in accordance with ASTM C1403-15. Concrete cubes were dried in an oven at 105 °C for 24 h and allowed to cool to room temperature prior to testing. These dried and cooled samples were then immersed in a water bath for 28 days. The water absorption, A_T (g/100 cm^2) was calculated using the following equation:

$$A_{28} = (W_{28} - W_0) \times 10{,}000/(L_1 \times L_2) \quad (1)$$

where W_{28} = the weight of the specimen at 28 days in grams, W_0 = the initial weight of the specimen in grams, L_1 = the average length of the test surface of the specimen cube in mm, and L_2 = the average width of the test surface of the specimen cube in mm.

The morphological and microstructural changes of specimen were studied with Scanning Electron Microscopy with Energy-Dispersive X-ray Spectroscopy (SEM-EDS. This technique combines the imaging capabilities of SEM to observe surface morphology with the elemental analysis capabilities of EDS to determine the chemical composition of the sample. A model Zeiss Supra 40 VP, operating with an accelerating potential ranging from 5 to 15 kV was used. Special attention was given to the interfacial transition zone (ITZ), which refers to the narrow region at the interface between the geopolymer binder matrix and the embedded particles such as aggregates or fillers. In this study, the ITZ was examined using SEM to assess morphological continuity (e.g., presence of cracks, voids, or gaps) and EDS to analyze elemental gradients, both of which provide insight into the effectiveness of the particle–matrix interaction. X-ray diffraction (XRD) was utilized to understand the composition and crystallinity changes of the specimen (Co Kα, Bruker D8 Advance). The scanning range is 15° to 60° 2θ, with voltage and current set at 40 kV and 15 mA, respectively. The resulting diffraction patterns were analyzed using Topas Academic v4 (Bruker), which employs non-linear least-squares Rietveld refinement and convolution-based peak profile fitting. This allowed for accurate separation of crystalline

and amorphous contributions, enabling reliable determination of the degree of crystallinity in each sample.

3. Results and Discussion

3.1. Phase Changes and Crystallinity Characterisation via XRD

To focus on the phase changes and compositional differences within the binder matrix of the specimens, a sieving process was conducted to retain particles smaller than 75 μm, effectively filtering out inert aggregates and isolating the reactive binder phases. This approach ensures that the analysis emphasizes the active components that contribute to hydration or geopolymerization processes. Figure 1 illustrates the phase changes observed in various binder systems, including Portland cement (C), fly ash (FA), slag (S), and fly ash-slag (FA + S) based geopolymer samples, from 7 to 28 days of curing. The primary crystalline phase detected in all samples is quartz (SiO_2), highlighted in gray for easier identification. The presence of quartz is likely due to its natural occurrence in the precursor materials or fine aggregates, even at particle sizes below 75 μm. Quartz acts as an inert filler that contributes positively to the mechanical properties of the binder matrix. Quartz crystalline nature provides structural reinforcement to the material by enhancing packing density and contributing to resistance against compressive forces, effectively improving the strength of the overall composite [35]. However, quartz particles are chemically inert under the conditions of both hydration and alkali activation, meaning they do not participate in the chemical reactions responsible for the formation of binding phases [36]. The results from this XRD analysis demonstrate differences of the hydration, geopolymerization, and hybrid reactions in different cementitious systems, in terms of the phases formed, their crystallinity, and their chemical composition. In the pure Portland cement system, the formation of C-S-H, CaOH and ettringite were evident, as expected from typical OPC hydration [37]. Clear peaks for C-S-H, portlandite and ettringite are clearly observed as labelled in Figure 1.

Unlike the products of cement hydration, the reaction products from geopolymerization are more challenging to identify due to their predominantly amorphous or poorly crystalline nature. Specifically, the primary reaction products—sodium or calcium aluminosilicate gels (N-A-S-H or C-A-S-H)—exhibit characteristic broad peaks instead of clear sharp peaks in the XRD spectra. Such broad band is noticeable in FA-based geopolymer, centered around 27° 2θ was observed. Previous studies have reported a similar broad peak for typical aluminosilicate geopolymer gels, typically located near 30–35° 2θ [38]. In contrast, the hump associated with raw fly ash powder appears at a lower 2θ angle, approximately 20° [39]. The broad hump observed in this study is thus interpreted as a combination of unreacted fly ash and the amorphous reaction products formed during geopolymerization. This interpretation arises from the partial overlap of the diffraction patterns of these two phases. Additionally, it is noteworthy that the XRD patterns of FA-based geopolymers show limited or absent peaks for traditional cement hydration products, such as portlandite and ettringite. The low calcium content in fly ash restricts the formation of calcium silicate hydrate (C-S-H) and portlandite, thereby favoring the production of N-A-S-H gel instead [40]. This lack of calcium availability explains the rare occurrence of portlandite peaks in the XRD patterns of pure fly ash-based geopolymers. Moreover, the analysis reveals peak corresponding to muscovite in the crystalline phase, which can be attributed to the components present in the raw fly ash.

Similarly, a broad hump was observed in the XRD pattern of the slag-based geopolymer; however, this hump was relatively narrower compared with that the fly ash-based geopolymer and was located at a higher 2θ value (approximately 35°). The presence of this broad peak indicates the formation of amorphous or poorly crystalline phases (N-A-S-H

and C-A-S-H), which are characteristic of the reaction products in geopolymer. Besides, the high calcium content in slag (compared to FA) plays a significant role in the development of binding phases within slag-based geopolymer systems [41]. In these environments, the calcium primarily contributes to the formation of C-S-H and C-A-S-H phases, rather than portlandite. This is primarily due to the high-alkaline conditions present during geopolymerization, which promote the dissolution of slag components [42]. The released calcium ions react readily with dissolved silicate species in the highly alkaline environment, driven by strong electrostatic attraction and the thermodynamic tendency to form low-energy, stable hydrates. This facilitates the rapid nucleation and growth of C-S-H or C-A-S-H gels [43]. In contrast to the hydration of OPC, where portlandite is a significant product, the limited availability of excess calcium ions in alkali-activated systems leads to less portlandite formation. Instead, the preferential reaction of calcium with silicates enhances the development of these hydrating gels, which contribute significantly to the mechanical properties and durability of the geopolymer. The low formation of portlandite in these systems is crucial as it indicates a shift in the binding mechanism from traditional hydration products to the formation of geopolymer gels, which are known for their long-term durability and strength [44]. The XRD spectra observed in this study support these findings, with notable peaks and broad humps corresponding to C-S-H and N-A-S-H/C-A-S-H phases.

In the case of a hybrid FA + S-based geopolymer, a broad hump was again observed, located at an identical 2θ value of approximately 35° compared with that of the slag-based geopolymer. Notably, the position of the broad hump in the FA-based geopolymer appeared in the low 2θ region, around 27°, indicating that fly ash remains largely unreactive in the pure FA-based system. However, the inclusion of slag significantly enhanced the geopolymerization reaction, demonstrating that the presence of slag alters the reaction kinetics in the pure fly ash-based geopolymer [34]. The increased concentration of calcium ions (Ca^{2+}) in the hybrid system facilitated the formation of typical hydration products such as C–S–H and ettringite, alongside the development of amorphous aluminosilicate gel. This indicates a coexistence of hydration and geopolymerization reactions in the complex hybrid matrix. The reactivity of fly ash in the presence of slag appears to be enhanced due to the altered ionic environment and increased alkalinity contributed by calcium-rich phases. Calcium ions not only promote early C–A–S–H gel formation, acting as nucleation sites, but also encourage further dissolution of fly ash by consuming silicates and sustaining ionic balance, thereby accelerating the geopolymerization process and product development [45,46]. Additionally, muscovite peaks were consistently observed in the FA-based geopolymer but disappeared in the 25FA + S-based geopolymer at 28 days of curing. This phenomenon suggests that muscovite crystals, which can dissolve in alkaline media, participated in the geopolymerization process [47]. The dissolution of these crystals highlights how the reactivity of fly ash is boosted in a more alkaline FA + S-based environment. Slag, containing a high content of calcium oxides (CaO), creates a strongly alkaline environment when dissolved in water. In contrast, fly ash primarily consists of amorphous aluminosilicate materials and contains low amounts of calcium, particularly in Class F fly ash. This reduced calcium content contributes to the relatively lower alkalinity of fly ash compared with slag. Consequently, the addition of slag not only enhances the overall reactivity of the geopolymer binder but also influences the structural development and mechanical performance of the final material.

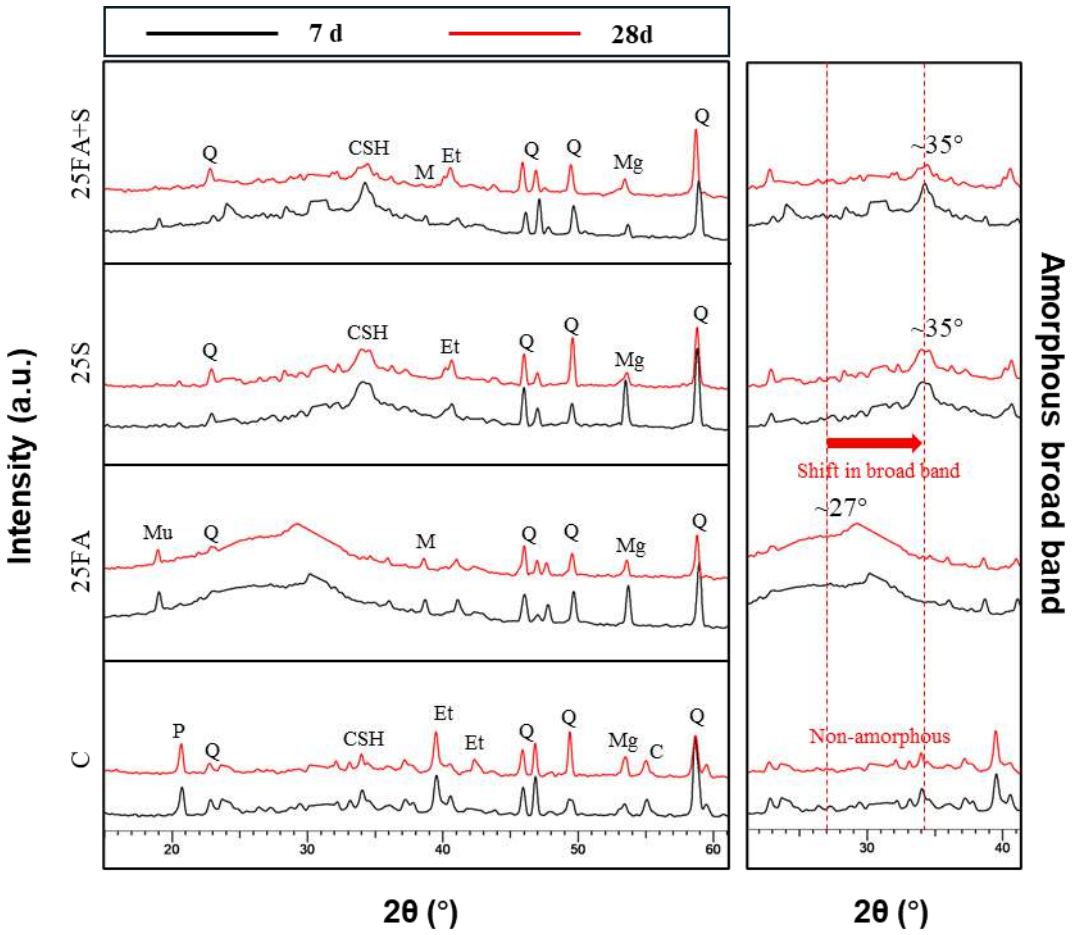

Figure 1. XRD patterns of C, 25FA, 25S and 25FA + S specimens illustrating their crystalline and amorphous changes at 7-day and 28-day. Amorphous broad band indicating the formation of aluminosilicate gel was labelled. [Q = Quartz; P = Portlandite, C = Calcite, CSH = Calcium Silicate Hydrate, Et = Ettringite, Mg = Magnetite, Mu = Muscovite, M = Mullite]. The peaks allocation was referred to [39,47,48].

Table 6 presents the variations in crystalline and amorphous content of the geopolymer specimens at both 7 and 28 days of curing. A comparative analysis between the 7-day and 28-day specimens reveals a general increase in crystallinity over time. This trend suggests that the geopolymerization reaction predominantly stabilizes by the 7-day mark, as indicated by the nearly unchanged broad hump in the XRD patterns. Following the 7-day period, the hydration reactions begin to play a more significant role, particularly in high-calcium geopolymer systems such as the 25S and 25FA + S mixtures. In these cases, the crystallinity of the specimens increased by approximately 6% by 28 days. This increase can be attributed to the continued reaction of the calcium ions released from the slag with silicate species, leading to the formation of crystalline phases, including C-S-H and ettringite [38]. Notably, the 25S sample exhibited the highest crystallinity at 7 days (25.9%) compared to 25FA (16.0%) and 25FA + S (19.1%), indicating more rapid early-stage phase formation, which correlates well with its superior early compressive strength. By 28 days, crystallinity further increased in 25S (to 31.7%) and 25FA + S (to 25.6%), reflecting continued structural development, whereas the FA-only system showed limited change, reinforcing its poor strength performance under ambient curing. This trend highlights the critical role of slag in promoting crystalline phase evolution due to its high calcium content and greater reactivity under alkaline conditions.

Table 6. Changes in crystalline and amorphous content of specimens at 7 days and 28 days. Quantitative crystallinity were determined by Topas Academic v4.

ID	Curing Age (d)	%-Crystallinity	%-Amorphous
25FA	7	16.0	84.0
	28	19.9	80.9
25S	7	25.9	74.1
	28	31.7	68.3
25FA + S	7	19.1	80.9
	28	25.6	74.4

While comparing the crystallinity across the specimen groups, it could be noticed that at 7 days, the 25S sample exhibited the highest crystallinity (25.9%) compared to 25FA (16.0%) and 25FA + S (19.1%), suggesting a more rapid early-stage reaction and phase formation. By 28 days, this crystallinity gap further widened, with 25S increasing to 31.7%, while 25FA + S rose to 25.6%, indicating continued structural development in systems with higher slag content. This trend highlights the critical influence of slag in promoting crystalline phase evolution due to its high calcium content and greater reactivity under alkaline activation. In contrast, fly ash is largely composed of amorphous aluminosilicate glass, which requires a longer activation period and typically contributes to the formation of amorphous or poorly crystalline geopolymer gels (e.g., N-A-S-H) [49]. The lower crystallinity observed in the FA-based system (25FA) is consistent with this, as geopolymerization tends to yield disordered three-dimensional aluminosilicate networks rather than well-defined crystalline structures. The slower dissolution of fly ash particles also delays the availability of reactive species, resulting in reduced early-stage phase development [50].

The increasing crystallinity observed in 25S and 25FA + S over time can be attributed to the formation of C-S-H and C-A-S-H-type hydration products, which are more crystalline in nature and typically arise from calcium-rich precursors like slag [45]. These phases form in parallel or in competition with geopolymer gels, particularly when slag is present in significant amounts. This shift toward a more crystalline binder matrix in slag-containing systems suggests that hydration-like reactions may dominate or complement geopolymerization, leading to denser and mechanically stronger microstructures. Therefore, the crystallinity trend across these mixtures reflects the interplay between geopolymerization (associated with amorphous gel formation) and hydration reactions (associated with crystalline phase formation).

3.2. Compressive Strength

Figure 2 illustrates the compressive strength of OPC control specimens, FA, S and FA + S-based geopolymer specimens at curing ages of 7 and 28 days. From Figure 2a, it was evident that the geopolymer system containing only FA exhibits the lowest performance. As the replacement ratio of FA increased, the compressive strength declined steeply. At a full replacement ratio (100% OPC replacement within the binder content), the achievable strength was negligible for 25FA, with a value of 0.35 MPa—representing only about 3% of the strength of the control specimen (12.44 MPa). This indicated that at low FA replacement levels, the compressive strength primarily originated from OPC hydration (e.g., C-S-H, ettringite, portlandite), with limited or no contribution from the geopolymerization process. Even at 28 days of curing, the compressive strength of the FA-based geopolymer showed only a slight improvement, reaching 1.22 MPa, which remained significantly lower than other specimens. The limited strength gain in FA-based geopolymers can be attributed to

the dependency of geopolymerization on thermal activation. The geopolymerization reaction of FA is highly temperature-sensitive, with the optimal curing temperature reported to be between 65–75 °C [51]. When FA-based geopolymers are cured at room temperature, as in this study, the reduced thermal energy limits the dissolution of aluminosilicate species, thus hindering the formation of the geopolymer matrix. Consequently, the formation of the aluminosilicate network remains incomplete, resulting in the observed poor mechanical properties. This is corroborated by XRD findings, where a broad hump centered around 27° 2θ was observed, indicating the presence of unreacted fly ash. The absence of crystalline hydration products such as portlandite and ettringite in FA-based binders also confirms limited calcium-driven phase formation, aligning with the weak mechanical performance. The trend of limited strength development in FA-based geopolymers cured at room temperature was reported in prior studies as well [34], where compressive strength values remained in the range of 1–2 MPa.

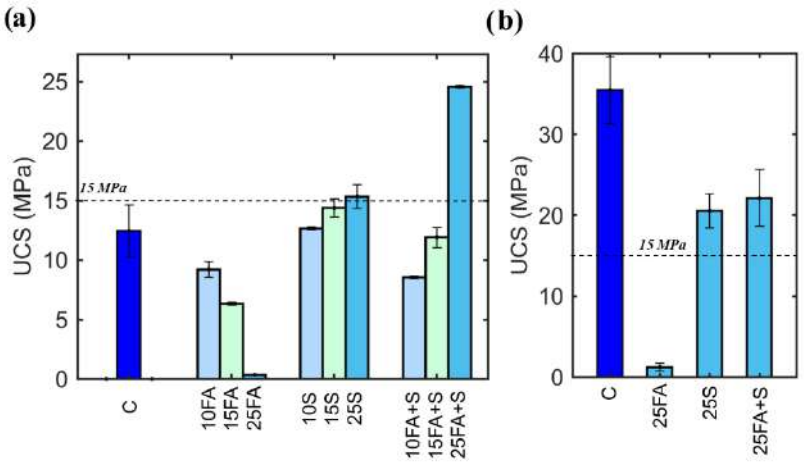

Figure 2. Unconfined Compressive Strength (UCS) results: (**a**) Comparison of control specimens and geopolymer specimens with varying precursor types and different substitution ratios of OPC at 7 days of curing; (**b**) Comparison of control specimens and 25FA, 25S and 25FA + S geopolymer specimens at 28 days of curing. Error bars represent the standard deviation. The horizontal line indicates the target compressive strength requirement for low-impact construction materials/single-story housing (15 MPa). Refer to Table 5 for detailed mix design of labelled binders.

For the slag-based geopolymer, the compressive strength at 7 days was found to be comparable to that of the control specimens. The strength gradually increased as the replacement ratio of OPC by slag increased, eventually surpassing the control specimens by approximately 16% when 100% replacement of OPC was achieved. This also meets the strength requirements for low-impact, single-story housing. Although room temperature curing is not ideal for slag-based geopolymer systems [52], their reactivity is significantly higher compared to fly ash-based geopolymers. As discussed in Section 3.1, the calcium content in slag plays a crucial role in increasing the pH when dissolved in an alkaline activator, which enhances the dissolution of aluminosilicate species and accelerates the geopolymerization process. This high alkalinity results in faster dissolution of reactive phases, releases calcium that reacts more readily at room temperature, forming strength-bearing products such as C-S-H and C-A-S-H, thereby facilitating setting and hardening. The slag-based geopolymer exhibits a hybrid reaction mechanism, where both hydration and geopolymerization occur simultaneously due to the higher calcium ion concentration compared with the FA-based geopolymer. The hydration reaction is driven by calcium ions, resulting in the formation of C-S-H, while the presence of sodium hydroxide in the system activates the aluminosilicate species, promoting geopolymerization. XRD spectra further support this dual-phase formation, showing a broad hump near 35° 2θ attributed to

amorphous C–A–S–H/N–A–S–H gels, along with minor crystalline peaks corresponding to C–S–H. The lack of portlandite in the spectra suggests calcium was efficiently utilized in gel formation rather than forming traditional hydration products. However, as the proportion of slag increases and OPC content is reduced, the system begins to shift from hydration-dominated reactions to the geopolymerization reaction. The observation that a geopolymerization-dominated system (e.g., 25S) can achieve greater early strength than a hydration-dominated system (e.g., 10S + 15OPC) implies that the reaction products of geopolymerization are inherently stronger than those from hydration. The aluminosilicate gel formed in geopolymerization (C-A-S-H and N-A-S-H) tends to produce a denser and more homogeneous matrix compared with the C-S-H produced through hydration. The geopolymer gel creates a highly cross-linked, three-dimensional network structure that enhances the material's mechanical integrity [44]. The dense network formed by the polymerization of silicate and aluminate species results in fewer voids and microcracks, which lowers the porosity and increases the overall compressive strength of the material.

A similar strength development trend was observed in the FA + S-based geopolymer system. At 7 days, the compressive strength was comparable to that of the control specimens. As the replacement ratio of OPC with FA + S increased, the strength continued to rise, ultimately surpassing the control specimens by 98% at full OPC replacement. This strength far exceeds the requirements for low-impact, single-story housing. These findings indicated that the enhanced dissolution and reactivity of fly ash in the presence of slag create a synergistic effect that allows the hybrid system to achieve greater strength compared with pure slag- or fly ash-based geopolymers. Yang et al. [38] also reported that binders synthesized with 100% GGBFS do not achieve the highest compressive strength compared with FA + S mixtures, suggesting that incorporating fly ash in the solid precursor positively contributes to maintaining superior macro-mechanical properties of alkali-silicate-activated binders. This synergy is reflected in the XRD pattern of the FA + S system, which shows a broad hump near 35° 2θ—similar to the slag system—but notably lacks the muscovite peak observed in the FA-based binder. This suggests active participation of aluminosilicate species in the reaction, confirming enhanced reactivity of FA when slag is present. Additionally, the co-existence of C–S–H, ettringite, and amorphous gels implies that both hydration and geopolymerization reactions occurred, contributing to the system's superior strength. In short, the early strength development in slag-based geopolymer systems (S and FA + S) is primarily attributed to the abundant availability of calcium ions from slag, which facilitates the rapid formation of C-A-S-H gels even under ambient curing, combined with enhanced geopolymerization due to the high alkalinity of the activator solution.

However, at the 28-day curing, both 25S and 25FA + S geopolymers demonstrated compressive strength lower than the control specimens. This can be explained by considering several factors related to microstructure development and shrinkage behavior. Geopolymer systems generally undergo relatively fast reaction kinetics compared to hydration in traditional Portland cement. This rapid reaction leads to the formation of a dense matrix at an early stage, which can hinder the continued reaction of any remaining unreacted precursors at the later age, which is particularly true for non-optimal room temperature curing of geopolymer system [53]. Once the activator solution is depleted, there may be insufficient driving force for further geopolymerization, resulting in unreacted particles being trapped within the matrix. These unreacted particles essentially act as weak points that limit strength development. This interpretation is consistent with the XRD findings, where the rate of crystallinity increase plateaued after 7 days, suggesting limited further structural evolution despite higher total crystallinity at 28 days. As a result, while initial strength may be comparable or even higher, the capacity for continued strength gain is

limited compared to traditional OPC systems that benefit from ongoing hydration reactions and densification over time.

Moreover, geopolymers are known to experience greater shrinkage compared with OPC systems [54]. This shrinkage is primarily driven by the rapid dissolution of precursors and the associated water loss during early-age reactions within the binder matrix. As a result, microcracks may form and progressively propagate, compromising the structural integrity over time. By 28 days, these shrinkage-induced microcracks can significantly reduce compressive strength by creating weak zones within the matrix. Evidence of such microcracking was clearly presented in Section 3.4, where the geopolymer specimens exhibited visible internal fissures indicative of drying shrinkage effects.

3.3. Water Absorption

Water absorption is primarily governed by the interconnectivity of capillaries within the concrete matrix [10]. A dense microstructure with few and small interconnected pores reduces water ingress, thereby enhancing durability. Low water absorption is indicative of better durability, as it limits the amount of water and potential contaminants entering the concrete through its porous structure.

Generally, water absorption properties exhibit a linear relationship with the mechanical properties of concrete specimens, as pore structure predominantly governs performance characteristics. However, in this study, it was noted that the control specimen exhibited the lowest water absorption among all samples (as shown in Figure 3), despite having lower compressive strength than the 25FA and 25FA + S geopolymer specimens at the 7-day curing age. Similar findings were reported by Ismail et al. (48); while alkali-activated binders exhibited higher mechanical strength, they had greater water absorption than OPC-based specimens, with increased FA content further increasing water absorption [55]. One possible factor contributing to this phenomenon is that fly ash and slag precursors typically are more water susceptible than OPC [56]. The fine particle size of fly ash increases its water demand due to its high surface area. Similarly, while slag has a slightly lower water demand compared with fly ash, its angular morphology and greater surface area result in higher water absorption than OPC. The irregular shape of slag particles contributes to a more complex pore structure, which can trap water within the concrete matrix.

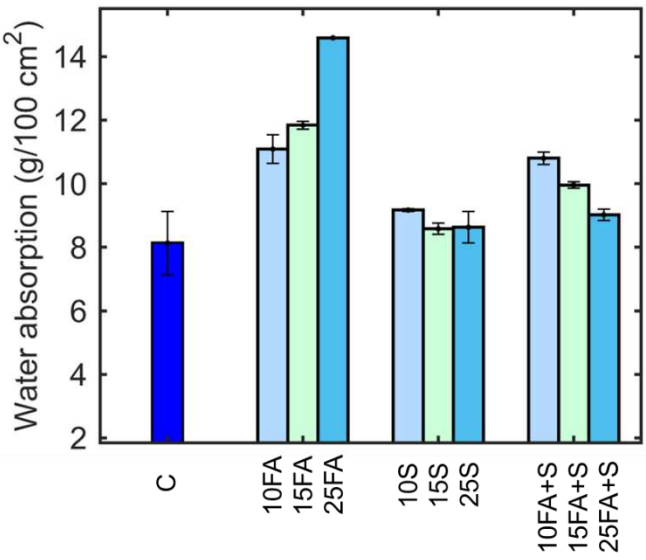

Figure 3. Water absorption of 7-day curing control samples C, and samples with varying precursor types and different substitution ratios.

In geopolymer systems, particularly those based on fly ash or slag, water absorption behavior is strongly influenced by both the extent of precursor activation and the type of reaction products formed. The increased water absorption observed in the geopolymer systems, particularly those containing fly ash, may be attributed to the presence of unreacted raw precursor materials. These unreacted particles tend to retain water, contributing to overall water absorption. Fly ash-based geopolymers, which form primarily N–A–S–H gels, are known to develop a less compact and more open gel network compared with C–A–S–H-rich matrices formed in slag-based systems. This difference in gel morphology can lead to higher pore interconnectivity in fly ash systems, enhancing capillary-driven absorption. It was observed that as the proportion of fly ash increased, water absorption correspondingly increased. Moreover, the FA + S geopolymer absorbed more water than the pure slag system, despite the 25FA + S mixture exhibiting higher strength and potentially better pore structure compared with the 25S system. This apparent contradiction may stem from the dual-phase nature of the FA + S system: while slag promotes dense C–A–S–H gel formation, the presence of partially unreacted fly ash particles and incomplete geopolymerization can result in microvoids or residual porosity, which increase water uptake. This can be explained by the presence of unreacted fly ash, which has a high-water demand and contributes to the overall absorption of water in the system. Additionally, from a practical standpoint, water absorption testing serves as a durability indicator for long-term exposure in moisture-rich environments. Higher absorption in FA-rich systems (which are not fully reacted and consumed) may not directly degrade mechanical performance but could influence dimensional stability and water permeability under immersion or fluctuating humidity conditions.

3.4. Microstructure

Figure 4 illustrates the interfacial transition zone (ITZ) between the binder system and the RPW, which is the microstructural region at the interface where the binder and aggregate interact physically and chemically, influencing strength and durability. In the OPC-based system, the RPW appears to act primarily as an inert filler, with minimal evidence of chemical interaction at the interface. This observation aligns with previous study [57], which have highlighted the chemically non-reactive nature of plastic waste in cementitious environments. The bonding at the ITZ in OPC matrices is predominantly physical and weak, often characterized by interfacial voids and poor adhesion. However, EDS analysis of the geopolymer system reveals enhanced interaction between the binder and the plastic aggregate, with notable presence of Ca, Si, and Al elements detected on the plastic surface. This improved interfacial behavior may be attributed to the highly alkaline environment of the geopolymer matrix, which can induce mild surface etching of plastic polymers, thereby improving mechanical interlocking and physical adhesion. These findings suggest that plastic waste aggregates exhibit better interfacial compatibility in alkali-activated systems compared to traditional OPC matrices.

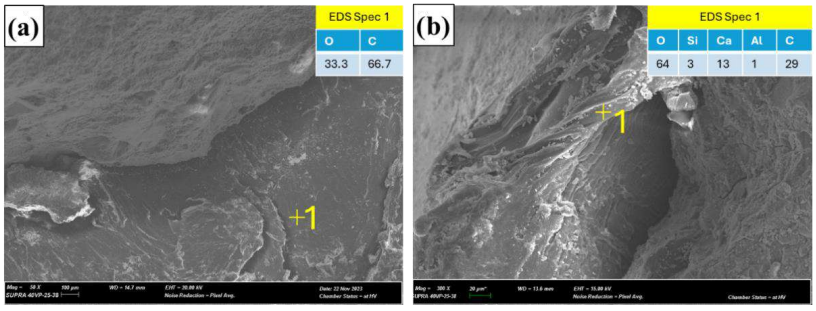

Figure 4. SEM-EDS analysis of the 28-day specimens: (**a**) control and (**b**) 25FA + S, illustrating the ITZ interactions between the binder system and the RPW. The EDS analysis reveals the presence of

carbon, confirming the incorporation of RPW within the binder matrix. Spot '1' indicates the location of the EDS analysis, with the corresponding results shown in the inset tables.

Figure 5 illustrates the ITZ interactions between the binder system and RCG, as well as the microcracks and reaction products observed in the control, 25FA, 25S, and 25FA + S concrete matrices at the 7-day curing age. In the control specimens, the ITZ appeared robust, with hydration reaction products effectively bonding with the aggregates, indicating good compatibility and strength development. In contrast, the 25S and 25FA + S specimens exhibited slight delamination at the ITZ, likely attributable to significant shrinkage cracking within the geopolymer matrix [58]. The presence of microcracks in the geopolymer matrix closely resembles observations by Brough et al. [59], who attributed similar cracking patterns to drying shrinkage effects in alkali-activated systems. From the SEM, it was shown that while the geopolymer matrix appears denser than that of the control specimens, it was also more susceptible to shrinkage-related damage. Notably, in the 25FA + S specimen, a substantial amount of unreacted or partially reacted spherical fly ash particles was evident [60], while the 25S geopolymer also contained some unreacted, angular slag components [61]. These observations highlight an incomplete geopolymerization reaction under the applied curing conditions, potentially resulting from inadequate heat or alkaline activation—an issue similarly noted by Duxson et al. [62], who emphasized the importance of optimizing activator concentration and curing temperature for full reaction development of geopolymer. Despite the presence of poor ITZ interactions, microcracks, and incomplete reactions, it was noteworthy that the 25S and 25FA + S geopolymers exhibited superior compressive strength relative to the control specimen. This suggests that the aluminosilicate gel network (C-A-S-H and/or N-A-S-H) formed during geopolymerization is intrinsically strong and capable of bridging localized flaws. It shows that geopolymer gels can exhibit high mechanical performance even with partial reactivity and heterogeneity in the microstructure. On the other hand, the matrix of the 25FA geopolymer appeared significantly powdery and filled with unreacted fly ash, resulting in a highly porous structure that lacked proper bonding. This morphology was consistent with the poor mechanical performance and high water absorption characteristics of this particular binder, highlighting the necessity for improved activation and curing conditions to enhance its reactivity and performance. The EDS analysis reveals higher concentrations of Al and Na ions in the geopolymer-based systems compared with the control specimens, indicating the formation of aluminosilicate gel. However, the low Na:Si ratio in the geopolymer mixes suggests limited N-A-S-H gel formation, possibly due to sodium ion depletion via alternate pathways, such as absorption by the aggregate surface or reaction into less desirable crystalline phases. This may result in a reduced effective liquid-to-powder (L/P) ratio, further limiting the extent of geopolymerization and increasing shrinkage susceptibility [63].

Figure 6 depicts the ITZ interactions between the binder matrix and RCG, as well as the microcracks and reaction products observed in the control, 25FA, 25S, and 25FA + S concrete matrices at 28 days of curing. Similarly, the ITZ in the control specimen appeared to have a more cohesive boundary layer and the overall matrix was denser and more homogeneous compared with the 7-day specimen. In the 25S specimen, the ITZ appeared better bonded at 28 days compared with the 7-day specimen, with noticeable improvements in the reduction of microcracks. The maximum crack width decreased from approximately 15 μm to 10 μm, suggesting a beneficial late-age filling effect from hydration products, which mitigated shrinkage cracks over time by filling the voids and improve bonding with aggregates. This observation is consistent with the findings of Brough et al. [59], who reported that microcracks gradually healed with extended curing age, attributed to ongoing hydration and the pore-filling effects of late-age geopolymerization. On the

other hand, the 25FA + S geopolymer system exhibited more severe delamination and an increase in the size and number of cracks at 28 days compared with the 7-day specimen. The maximum crack size increased from 5 µm to 12 µm, indicating that the geopolymer matrix failed to compensate for shrinkage-related stresses effectively. The 25FA + S system, due to the presence of low-calcium FA, is governed more by geopolymerization rather than hydration. The worsening ITZ at the curing stage suggests that geopolymerization did not adequately fill gaps or provide strong binding at the ITZ, which corroborates the earlier discussion in Section 3.2 regarding insufficient late-stage densification in FA-containing systems. The weaker ITZ and increased cracking in the FA-containing geopolymer systems likely contribute to reduced load-transfer efficiency between the matrix and aggregates, negatively impacting the overall compressive strength [64]. SEM analysis further revealed that unreacted fly ash and slag particles not only failed to act as effective fillers but also served as weak points in the binder matrix [65]. These unreacted particles were often surrounded by cracks, forming poorly bonded interfaces with the gel matrix, which acted as sources of failure. This observation was consistent with the compressive strength results, where a slight decline in strength was recorded for the 25FA + S system from 7 days to 28 days. The inability of the system to develop sufficient late-age strength through geopolymerization, coupled with increased cracking, led to an overall deterioration in its mechanical properties. Regarding the 25FA geopolymer, the matrix still exhibited a powdery appearance with numerous unreacted fly ash particles, indicating incomplete reaction. The porous structure observed suggested that the geopolymerization process remained ineffective not only during the early stages but also throughout the later stages of curing in the pure FA system, resulting in insufficient matrix densification and poor mechanical integrity.

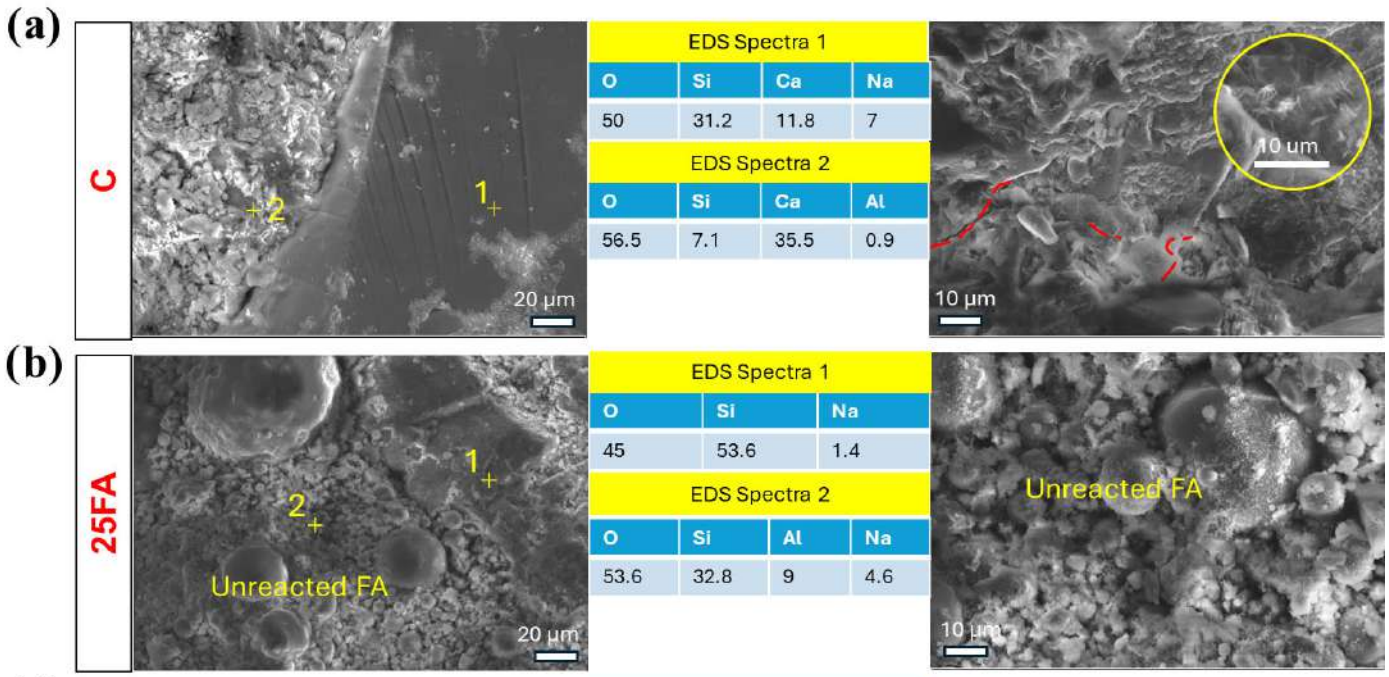

Figure 5. *Cont.*

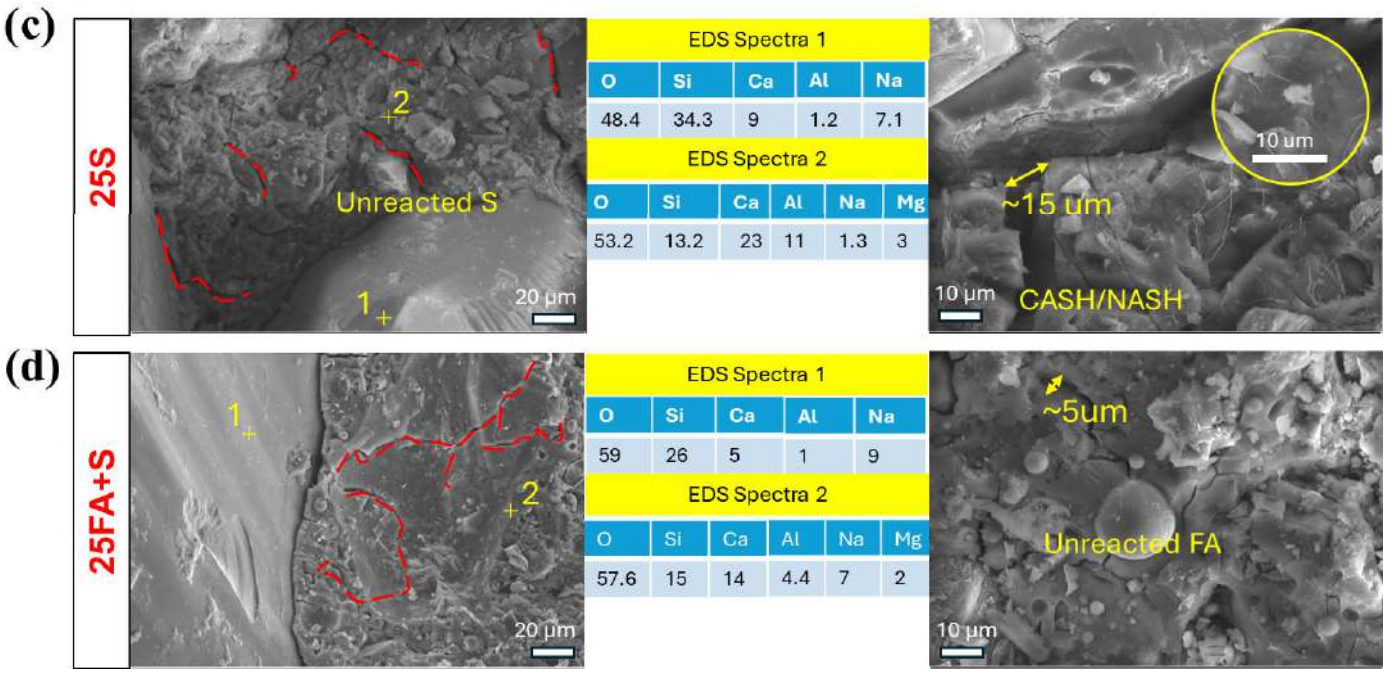

Figure 5. SEM-EDS analysis of the 7-day specimens: (**a**) control (C), (**b**) 25FA, (**c**) 25S, and (**d**) 25FA + S. Crack propagation is highlighted with red dotted lines. The left-hand side SEM images illustrate the interfacial transition zone (ITZ) interactions between the recycled glass aggregate and the binder matrix. The yellow circle insets in (**a**,**c**) highlighted the presence of hydration products (C-S-H and ettringite). Red-dotted lines highlight the cracking paths within the matrix. Spots labelled '1' and '2' mark the locations of EDS analysis, with corresponding elemental compositions presented in the inset EDS tables.

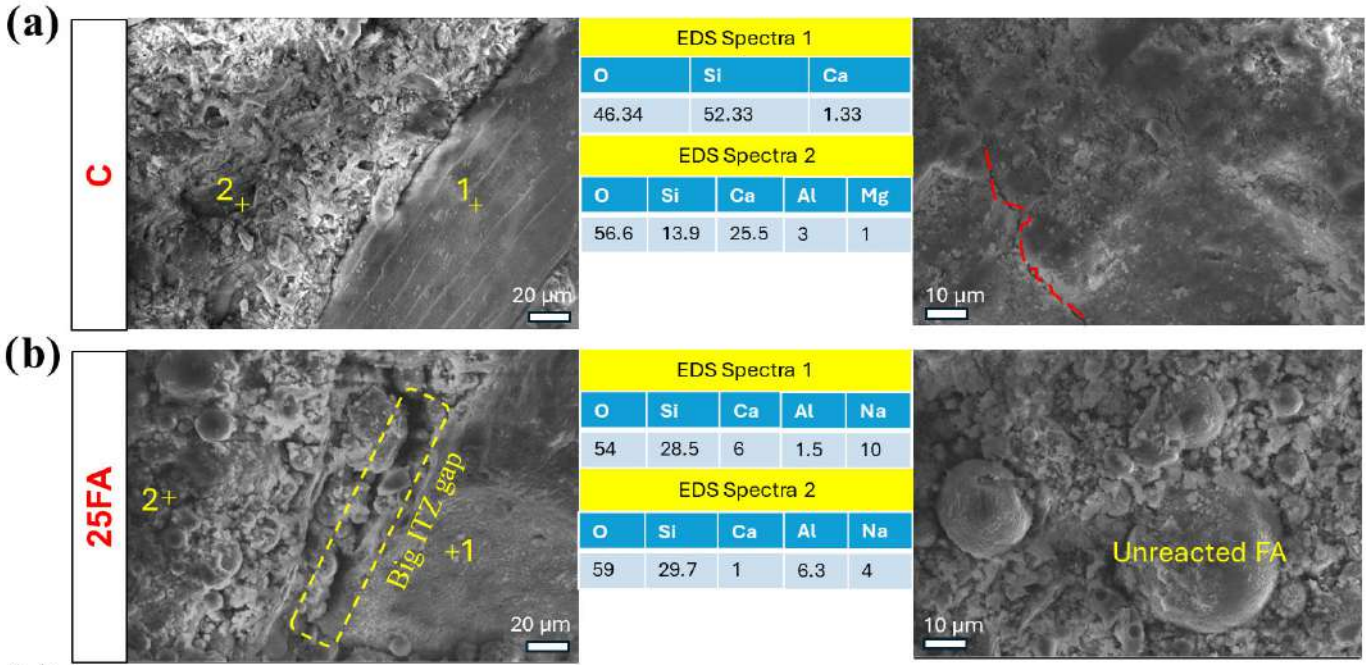

Figure 6. *Cont.*

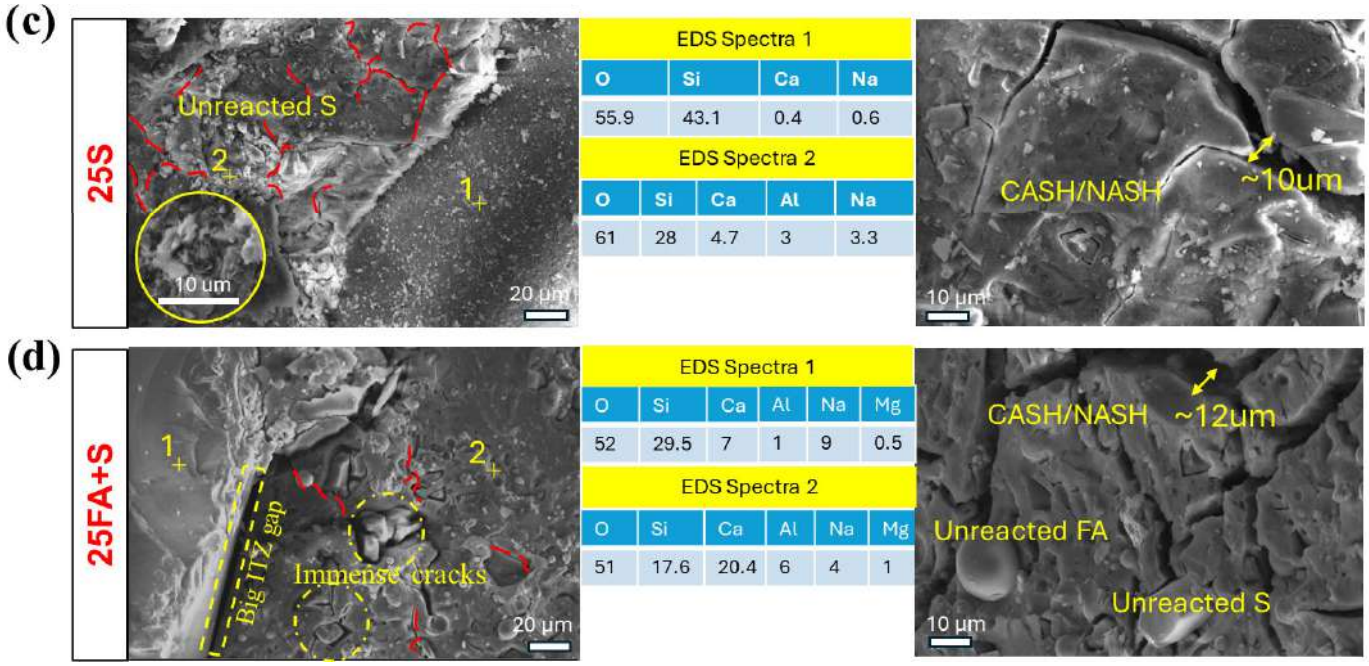

Figure 6. SEM-EDS analysis of the 28-day specimens: (**a**) control (C), (**b**) 25FA, (**c**) 25S, and (**d**) 25FA + S. Crack propagation is highlighted with red dotted lines. The left-hand side SEM images illustrate the interfacial transition zone (ITZ) interactions between the recycled glass aggregate and the binder matrix. The yellow circle inset in (**c**) highlighted the presence of hydration products (C-S-H and ettringite). Red-dotted lines highlight the cracking paths within the matrix. Spots labelled '1' and '2' mark the locations of EDS analysis, with corresponding elemental compositions presented in the inset EDS tables.

4. Conclusions

In conclusion, this study demonstrates the viability of FA, S, and FA + S-based geopolymers, combined with RPW and RCG, as sustainable alternatives to OPC for low-cost housing construction. Mechanical testing revealed that the 25% (FA + S) geopolymer mixture achieved the highest early strength of 24.6 MPa at 7 days, which is 98% higher than control specimen. Water absorption results indicated that the slag-based geopolymer specimens demonstrated comparable performances to OPC samples. This confirms the potential for full OPC replacement using geopolymers entirely derived from industrial by-products. SEM-EDS and XRD analyses confirmed the presence of a dense microstructure in FA + S and S-based geopolymers, along with improved interfacial bonding with recycled plastic aggregates. This improvement is attributed to the highly alkaline geopolymer matrix, which induces mild surface etching of the plastic, thereby promoting mechanical interlocking at the interface. While glass aggregates initially exhibited good compatibility with the geopolymer binder, signs of ITZ delamination were observed at later ages, likely due to the severe shrinkage stresses developed during the geopolymerization process. On the other hand, these analyses also identified incomplete geopolymerization, as evidenced by unreacted FA and S particles, along with extensive shrinkage-driven cracking. These findings highlight the need for improved curing conditions to prevent moisture loss and mitigate shrinkage-induced cracking. Despite these challenges, the geopolymers met the performance criteria for construction applications. While the beneficial effect of slag on enhancing reactivity is well recognized, this study specifically demonstrates that slag addition not only accelerated early strength development but also promoted continuous structural densification and crystallinity over time under ambient curing. At early ages, hydration-driven reactions dominated, leading to the rapid formation of C-S-H and C-A-S-H gels. As curing progressed, ongoing geopolymerization and further reaction of residual amorphous

phases contributed to additional crystallization and microstructural refinement, resulting in a denser and more durable binder matrix. This study underscores the environmental benefits of replacing OPC with geopolymers, which utilize industrial by-products like fly ash and slag to offer a low-carbon alternative to conventional cement. The incorporation of waste-derived aggregates such as crushed plastic and glass further supports sustainable resource use and waste reduction. The observed microstructural interactions emphasize the feasibility of combining recycled materials with geopolymer binders, provided that compatibility at the interfacial level is carefully managed through mix design and curing strategies. By integrating geopolymers with recycled materials, this approach promotes a circular economy model, particularly suited for developing regions seeking affordable and durable construction solutions. Slag- and FA + S-based geopolymers achieved over 15 MPa compressive strength within 7 days and maintained values above this threshold after 28 days, meeting the requirements for low-rise housing. Future work should explore the long-term durability of these systems under aggressive environmental conditions.

Author Contributions: Conceptualization, Y.C.W. and E.K.M.; Methodology, Z.Q.T. and Y.C.W.; Validation, Z.Q.T. and Y.C.W.; Formal Analysis, Z.Q.T.; Resources, Y.L. and Y.C.W.; Writing—Original Draft Preparation, Z.Q.T. and Y.L.; Writing—Review & Editing, Z.Q.T. and Y.L.; Supervision, Y.C.W. and E.K.M.; Project Administration, Y.C.W. and E.K.M.; Funding Acquisition, Y.C.W. and Y.L. All authors have read and agreed to the published version of the manuscript.

Funding: This research was funded by the Swinburne Research Ecosystem Seed Grant (Grant No. RMC-3477) and the Australian Research Council (Grant No. FT200100985).

Data Availability Statement: The raw data supporting the conclusions of this article will be made available by the authors on request.

Acknowledgments: This work was supported by the Swinburne Research Ecosystem Seed Grant (RMC-3477). The authors would like to thank ACT Pty Ltd. for the support in this project. The authors are sincerely grateful for the financial support from the Australian Research Council through Future Fellowship grant FT200100985 in conducting this study.

Conflicts of Interest: The authors declare that they have no known competing financial interests or personal relationships that could have appeared to influence the work reported in this paper.

References

1. Makinde, O.O. Housing: Central city slums, a case study of Ibadan. *J. Environ. Earth Sci.* **2012**, *2*, 21–31.
2. Chowdhury, R.B.; Moore, G.A. Floating agriculture: A potential cleaner production technique for climate change adaptation and sustainable community development in Bangladesh. *J. Clean. Prod.* **2017**, *150*, 371–389. [CrossRef]
3. Adabre, M.A.; Chan, A.P.; Darko, A.; Osei-Kyei, R.; Abidoye, R.; Adjei-Kumi, T. Critical barriers to sustainability attainment in affordable housing: International construction professionals' perspective. *J. Clean. Prod.* **2020**, *253*, 119995. [CrossRef]
4. Rahmawati, D.; Rahadi, R.A.; Putri, A.D.; Bandung, E. The Current State of Property Development in Indonesia During the Covid-19 Pandemic. *Int. J. Innov. Creat. Change* **2021**, *15*, 2021.
5. Satoto, E.B. Boosting Homeownership Affordability for Low-Income Communities in Indonesia. *Int. J. Sustain. Dev. Plan.* **2023**, *18*, 1365–1376. [CrossRef]
6. Odoyi, E.J.; Riekkinen, K. Housing policy: An analysis of public housing policy strategies for low-income earners in Nigeria. *Sustainability* **2022**, *14*, 2258. [CrossRef]
7. Ebekozien, A.; Abdul-Aziz, A.-R.; Jaafar, M. Low-cost housing policies and squatters struggles in Nigeria: The Nigerian perspective on possible solutions. *Int. J. Constr. Manag.* **2021**, *21*, 1088–1098. [CrossRef]
8. Purnamasari, L. Effect of Government's Policy to Build 1 Million Houses on Performance of Housing and Apartment Credits of Banks Listed in Indonesia Stock Exchange During Period 2015–2017. *J. Ilm. Ilmu Adm. Publik* **2021**, *11*, 40–50. [CrossRef]
9. Zuraida, S.; Dewancker, B.; Margono, R.B. Application of non-degradable waste as building material for low-cost housing. *Sci. Rep.* **2023**, *13*, 6390. [CrossRef]

10. Shamsaei, E.; Tang, Z.Q.; de Souza, F.B.; Hosseini, E.; Benhelal, E.; Korayem, A.H.; Duan, W. Zeolitic imidazolate framework nanoleaves (ZIF-L) enhancement of strength and durability of portland cement composites. *Constr. Build. Mater.* **2021**, *272*, 122015. [CrossRef]
11. Davidovits, J. Geopolymers: Inorganic polymeric new materials. *J. Therm. Anal. Calorim.* **1991**, *37*, 1633–1656. [CrossRef]
12. McLellan, B.C.; Williams, R.P.; Lay, J.; Van Riessen, A.; Corder, G.D. Costs and carbon emissions for geopolymer pastes in comparison to ordinary portland cement. *J. Clean. Prod.* **2011**, *19*, 1080–1090. [CrossRef]
13. Vafaei, M.; Allahverdi, A. Strength development and acid resistance of geopolymer based on waste clay brick powder and phosphorous slag. *Struct. Concr.* **2019**, *20*, 1596–1606. [CrossRef]
14. Akhtar, N.; Ahmad, T.; Husain, D.; Majdi, A.; Alam, M.T.; Husain, N.; Wayal, A.K.S. Ecological footprint and economic assessment of conventional and geopolymer concrete for sustainable construction. *J. Clean. Prod.* **2022**, *380*, 134910. [CrossRef]
15. Rintala, A.; Havukainen, J.; Abdulkareem, M. Estimating the cost-competitiveness of recycling-based geopolymer concretes. *Recycling* **2021**, *6*, 46. [CrossRef]
16. Khan, M.N.N.; Saha, A.K.; Sarker, P.K. Reuse of waste glass as a supplementary binder and aggregate for sustainable cement-based construction materials: A review. *J. Build. Eng.* **2020**, *28*, 101052. [CrossRef]
17. Luhar, S.; Cheng, T.-W.; Nicolaides, D.; Luhar, I.; Panias, D.; Sakkas, K. Valorisation of glass waste for development of Geopolymer composites–Mechanical properties and rheological characteristics: A review. *Constr. Build. Mater.* **2019**, *220*, 547–564. [CrossRef]
18. Qian, Y.; Sheikh, M.N.; Feng, H.; Hadi, M.N. Use of waste glass as fine aggregate in ambient cured alkali-activated mortars. *Struct. Concr.* **2023**, *24*, 4145–4160. [CrossRef]
19. Torres-Carrasco, M.; Puertas, F. Waste glass in the geopolymer preparation. Mechanical and microstructural characterisation. *J. Clean. Prod.* **2015**, *90*, 397–408. [CrossRef]
20. Puertas, F.; Torres-Carrasco, M. Use of glass waste as an activator in the preparation of alkali-activated slag. Mechanical strength and paste characterisation. *Cem. Concr. Res.* **2014**, *57*, 95–104. [CrossRef]
21. Tapas, M.J.; Thomas, P.; Vessalas, K.; Nsiah-Baafi, E.; Martin, L.; Sirivivatnanon, V. Comparative study of the efficacy of fly ash and reactive aggregate powders in mitigating alkali-silica reaction. *J. Build. Eng.* **2023**, *63*, 105571. [CrossRef]
22. Lei, J.; Fu, J.; Yang, E.-H. Alkali-silica reaction resistance and pore solution composition of low-calcium fly ash-based geopolymer concrete. *Infrastructures* **2020**, *5*, 96. [CrossRef]
23. Neo, E.R.K.; Soo, G.C.Y.; Tan, D.Z.L.; Cady, K.; Tong, K.T.; Low, J.S.C. Life cycle assessment of plastic waste end-of-life for India and Indonesia. *Resour. Conserv. Recycl.* **2021**, *174*, 105774. [CrossRef]
24. Darus, N.; Tamimi, M.; Tirawaty, S.; Muchtazar, M.; Trisyanti, D.; Akib, R.; Condorini, D.; Ranggi, K. An overview of plastic waste recycling in the urban areas of Java Island in Indonesia. *J. Environ. Sci. Sustain. Dev.* **2020**, *3*, 402–415. [CrossRef]
25. Pawar, P.R.; Shirgaonkar, S.S.; Patil, R.B. Plastic marine debris: Sources, distribution and impacts on coastal and ocean biodiversity. *PENCIL Publ. Biol. Sci.* **2016**, *3*, 40–54.
26. Campanale, C.; Massarelli, C.; Savino, I.; Locaputo, V.; Uricchio, V.F. A detailed review study on potential effects of microplastics and additives of concern on human health. *Int. J. Environ. Res. Public Health* **2020**, *17*, 1212. [CrossRef]
27. Al-Tulaian, B.; Al-Shannag, M.; Al-Hozaimy, A. Recycled plastic waste fibers for reinforcing Portland cement mortar. *Constr. Build. Mater.* **2016**, *127*, 102–110. [CrossRef]
28. Asokan, P.; Osmani, M.; Price, A.D. Assessing the recycling potential of glass fibre reinforced plastic waste in concrete and cement composites. *J. Clean. Prod.* **2009**, *17*, 821–829. [CrossRef]
29. Silva, R.V.; de Brito, J.; Saikia, N. Influence of curing conditions on the durability-related performance of concrete made with selected plastic waste aggregates. *Cem. Concr. Compos.* **2013**, *35*, 23–31. [CrossRef]
30. Ferreira, L.; De Brito, J.; Saikia, N. Influence of curing conditions on the mechanical performance of concrete containing recycled plastic aggregate. *Constr. Build. Mater.* **2012**, *36*, 196–204. [CrossRef]
31. Mohammadinia, A.; Wong, Y.C.; Arulrajah, A.; Horpibulsuk, S. Strength evaluation of utilizing recycled plastic waste and recycled crushed glass in concrete footpaths. *Constr. Build. Mater.* **2019**, *197*, 489–496. [CrossRef]
32. Wong, Y.C.; Perera, S.; Zhang, Z.; Arulrajah, A.; Mohammadinia, A. Field study on concrete footpath with recycled plastic and crushed glass as filler materials. *Constr. Build. Mater.* **2020**, *243*, 118277. [CrossRef]
33. Sing, M.; Love, P.; Tam, C.-M. Review and exploration of river sand substitutes for concrete production in Asian countries. In *Advances in Civil Engineering and Building Materials*; CRC Press: Boca Raton, FL, USA, 2012; pp. 115–117.
34. Arulrajah, A.; Perera, S.; Wong, Y.C.; Maghool, F.; Horpibulsuk, S. Stabilization of PET plastic-demolition waste blends using fly ash and slag-based geopolymers in light traffic road bases/subbases. *Constr. Build. Mater.* **2021**, *284*, 122809. [CrossRef]
35. Kang, S.-H.; Jeong, Y.; Tan, K.H.; Moon, J. The use of limestone to replace physical filler of quartz powder in UHPFRC. *Cem. Concr. Compos.* **2018**, *94*, 238–247. [CrossRef]
36. Tang, Z.Q.; Sui, H.; de Souza, F.B.; Sagoe-Crentsil, K.; Duan, W. Silane-modified graphene oxide in geopolymer: Reaction kinetics, microstructure, and mechanical performance. *Cem. Concr. Compos.* **2023**, *139*, 104997. [CrossRef]

37. Bullard, J.W.; Jennings, H.M.; Livingston, R.A.; Nonat, A.; Scherer, G.W.; Schweitzer, J.S.; Scrivener, K.L.; Thomas, J.J. Mechanisms of cement hydration. *Cem. Concr. Res.* **2011**, *41*, 1208–1223. [CrossRef]
38. Yang, T.; Yao, X.; Zhang, Z.; Wang, H. Mechanical property and structure of alkali-activated fly ash and slag blends. *J. Sustain. Cem.-Based Mater.* **2012**, *1*, 167–178. [CrossRef]
39. Singh, G.B.; Subramaniam, K.V. Quantitative XRD study of amorphous phase in alkali activated low calcium siliceous fly ash. *Constr. Build. Mater.* **2016**, *124*, 139–147. [CrossRef]
40. Moujoud, Z.; Sair, S.; Ousaleh, H.A.; Amadine, O.; Ayouch, I.; Zahouily, M.; El Bouari, A.; Tanane, O. High-performance geopolymer from brick wastes and metakaolin: Alkali treatment optimization, phase transformation, and property analysis. *Struct. Concr.* **2024**, *26*, 1477–1497. [CrossRef]
41. Bourzik, O.; Baba, K.; Akkouri, N. Eco-friendly geopolymer mortar prepared from geopolymer waste: Mechanical and thermal properties. *Environ. Qual. Manag.* **2024**, *33*, 411–419. [CrossRef]
42. Zhu, X.; Luan, M.; Tang, D.; Yang, K.; Yang, C. Understanding the setting behaviours of alkali-activated slag from the dissolution-precipitation point of view. *Cem. Concr. Compos.* **2024**, *148*, 105474. [CrossRef]
43. Hu, Y.; Shao, Z.; Wang, J.; Zang, J.; Tang, L.; Ma, F.; Qian, B.; Ma, B.; Wang, L. Investigation into the influence of calcium compounds on the properties of micropore-foamed geopolymer. *J. Build. Eng.* **2022**, *45*, 103521. [CrossRef]
44. Tailby, J.; MacKenzie, K.J. Structure and mechanical properties of aluminosilicate geopolymer composites with Portland cement and its constituent minerals. *Cem. Concr. Res.* **2010**, *40*, 787–794. [CrossRef]
45. Puligilla, S.; Mondal, P. Role of slag in microstructural development and hardening of fly ash-slag geopolymer. *Cem. Concr. Res.* **2013**, *43*, 70–80. [CrossRef]
46. Sanalkumar, K.U.A.; Lahoti, M.; Yang, E.-H. Investigating the potential reactivity of fly ash for geopolymerization. *Constr. Build. Mater.* **2019**, *225*, 283–291. [CrossRef]
47. Tang, Z.Q.; De Souza, F.B.; Mulder, R.J.; Duan, W. Multistep nucleation and growth mechanism of aluminosilicate gel observed by cryo-electron microscopy. *Cem. Concr. Res.* **2022**, *159*, 106873. [CrossRef]
48. Lecomte, I.; Henrist, C.; Liégeois, M.; Maseri, F.; Rulmont, A.; Cloots, R. (Micro)-structural comparison between geopolymers, alkali-activated slag cement and Portland cement. *J. Eur. Ceram. Soc.* **2006**, *26*, 3789–3797. [CrossRef]
49. Lee, B.; Kim, G.; Kim, R.; Cho, B.; Lee, S.; Chon, C.-M. Strength development properties of geopolymer paste and mortar with respect to amorphous Si/Al ratio of fly ash. *Constr. Build. Mater.* **2017**, *151*, 512–519. [CrossRef]
50. Fernández-Jiménez, A.; Palomo, A.; Criado, M. Microstructure development of alkali-activated fly ash cement: A descriptive model. *Cem. Concr. Res.* **2005**, *35*, 1204–1209. [CrossRef]
51. Sukmak, P.; Horpibulsuk, S.; Shen, S.-L. Strength development in clay–fly ash geopolymer. *Constr. Build. Mater.* **2013**, *40*, 566–574. [CrossRef]
52. Saludung, A.; Azeyanagi, T.; Ogawa, Y.; Kawai, K. Mechanical and microstructural evolutions of fly ash/slag-based geopolymer at high temperatures: Effect of curing conditions. *Ceram. Int.* **2023**, *49*, 2091–2101. [CrossRef]
53. Ranjbar, N.; Kuenzel, C.; Spangenberg, J.; Mehrali, M. Hardening evolution of geopolymers from setting to equilibrium: A review. *Cem. Concr. Compos.* **2020**, *114*, 103729. [CrossRef]
54. Zhang, B.; Zhu, H.; Feng, P.; Zhang, P. A review on shrinkage-reducing methods and mechanisms of alkali-activated/geopolymer systems: Effects of chemical additives. *J. Build. Eng.* **2022**, *49*, 104056. [CrossRef]
55. Ismail, I.; Bernal, S.A.; Provis, J.L.; San Nicolas, R.; Brice, D.G.; Kilcullen, A.R.; Hamdan, S.; van Deventer, J.S. Influence of fly ash on the water and chloride permeability of alkali-activated slag mortars and concretes. *Constr. Build. Mater.* **2013**, *48*, 1187–1201. [CrossRef]
56. Giergiczny, Z. Fly ash and slag. *Cem. Concr. Res.* **2019**, *124*, 105826. [CrossRef]
57. Thorneycroft, J.; Orr, J.; Savoikar, P.; Ball, R. Performance of structural concrete with recycled plastic waste as a partial replacement for sand. *Constr. Build. Mater.* **2018**, *161*, 63–69. [CrossRef]
58. Liu, Y.; Wei, Y.; Ma, L.; Wang, L. Restrained shrinkage behavior of internally-cured UHPC using calcined bauxite aggregate in the ring test and UHPC-concrete composite slab. *Cem. Concr. Compos.* **2022**, *134*, 104805. [CrossRef]
59. Brough, A.; Atkinson, A. Sodium silicate-based, alkali-activated slag mortars: Part I. Strength, hydration and microstructure. *Cem. Concr. Res.* **2002**, *32*, 865–879. [CrossRef]
60. Klima, K.; Schollbach, K.; Brouwers, H.; Yu, Q. Enhancing the thermal performance of Class F fly ash-based geopolymer by sodalite. *Constr. Build. Mater.* **2022**, *314*, 125574. [CrossRef]
61. Kalinkin, A.; Kumar, S.; Gurevich, B.; Alex, T.; Kalinkina, E.; Tyukavkina, V.; Kalinnikov, V.; Kumar, R. Geopolymerization behavior of Cu–Ni slag mechanically activated in air and in CO_2 atmosphere. *Int. J. Miner. Process.* **2012**, *112*, 101–106. [CrossRef]
62. Duxson, P.; Fernández-Jiménez, A.; Provis, J.L.; Lukey, G.C.; Palomo, A.; van Deventer, J.S. Geopolymer technology: The current state of the art. *J. Mater. Sci.* **2007**, *42*, 2917–2933. [CrossRef]
63. Singh, B.; Rahman, M.R.; Paswan, R.; Bhattacharyya, S. Effect of activator concentration on the strength, ITZ and drying shrinkage of fly ash/slag geopolymer concrete. *Constr. Build. Mater.* **2016**, *118*, 171–179. [CrossRef]

64. He, S.; Yang, E.-H. Strategic strengthening of the interfacial transition zone (ITZ) between microfiber and cement paste matrix with carbon nanofibers (CNFs). *Cem. Concr. Compos.* **2021**, *119*, 104019. [CrossRef]
65. Khodr, M.; Law, D.W.; Gunasekara, C.; Setunge, S.; Brkljaca, R. Compressive strength and microstructure evolution of low calcium brown coal fly ash-based geopolymer. *J. Sustain. Cem.-Based Mater.* **2020**, *9*, 17–34. [CrossRef]